# Supplementary Materials for

# Neural basis of opioid-induced respiratory depression and its rescue

Shijia Liu[1,2], Dongil Kim[1], Tae Gyu Oh[3], Gerald Pao[4], Jonghyun Kim[1], Richard D. Palmiter[5], Matthew R. Banghart[2], Kuo-Fen Lee[1,2], Ronald M. Evans[3], Sung Han[1,2,*]

[1]Peptide Biology Laboratories, The Salk Institute for Biological Studies, La Jolla, CA 92037, USA.
[2] Section of Neurobiology, Division of Biological Sciences, University of California, San Diego, La Jolla, CA 92093, USA.
[3]Howard Hughes Medical Institute, Gene Expression Laboratories, The Salk Institute for Biological Studies, La Jolla, CA 92037, USA.
[4]Molecular and Cellular Biology Laboratories, The Salk Institute for Biological Studies, La Jolla, CA 92037, USA.
[5]Howard Hughes Medical Institute, Department of Biochemistry, School of Medicine, University of Washington, Seattle, WA 98195, USA.
*Corresponding author. Email: sunghan@salk.edu.

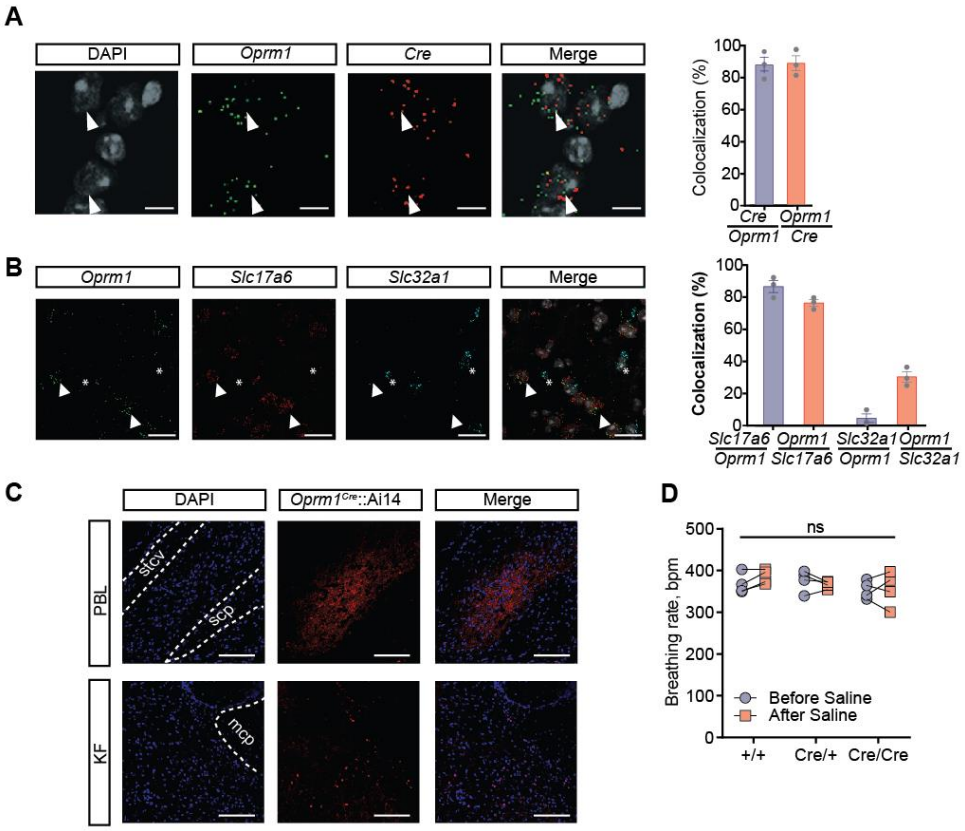


**Figure S1.** Characterization of the *Oprm1*$^{Cre}$ mouse line and PBL$^{Oprm1}$ neurons. (**A**) RNA *in situ* hybridization and quantification of the colocalization for *Oprm1* and *Cre* mRNAs in the PBL of *Oprm1*$^{Cre/+}$ mice (n = 902 cells from 3 animals). Arrowheads, double-labeled cells. Scale bar, 10 µm. (**B**) RNA *in situ* hybridization and quantification of the colocalization for *Oprm1*, *Slc17a6* (encoding VGLUT2), and *Slc32a1* (encoding VGAT) mRNAs in the PBL of wild type mice (n = 1552 and 1431 cells from 3 animals). Arrowheads, *Oprm1*$^{+}$ / *Slc17a6*$^{+}$ cells; asterisks, *Oprm1*$^{-}$ / *Slc32a1*$^{+}$ cells. Scale bar, 50 µm. (**C**) Example histology from *Oprm1*$^{Cre}$*::*Ai14 double transgenic mice showing tdTomato expression in the PBL and KF under the same microscope settings. Anatomical landmarks for PBL: stcv, ventral spinocerebellar tract; scp, superior cerebellar peduncle; mcp, middle cerebellar peduncle. Scale bar, 200 µm. (**D**) *Oprm1*$^{Cre}$ mice do not exhibit baseline breathing differences compared to the wild type mice. Breathing rate before and after saline injection did not display considerable differences across genotypes and within each genotype. Two-way ANOVA with Bonferroni's multiple comparison post-hoc test. ns, not significant.

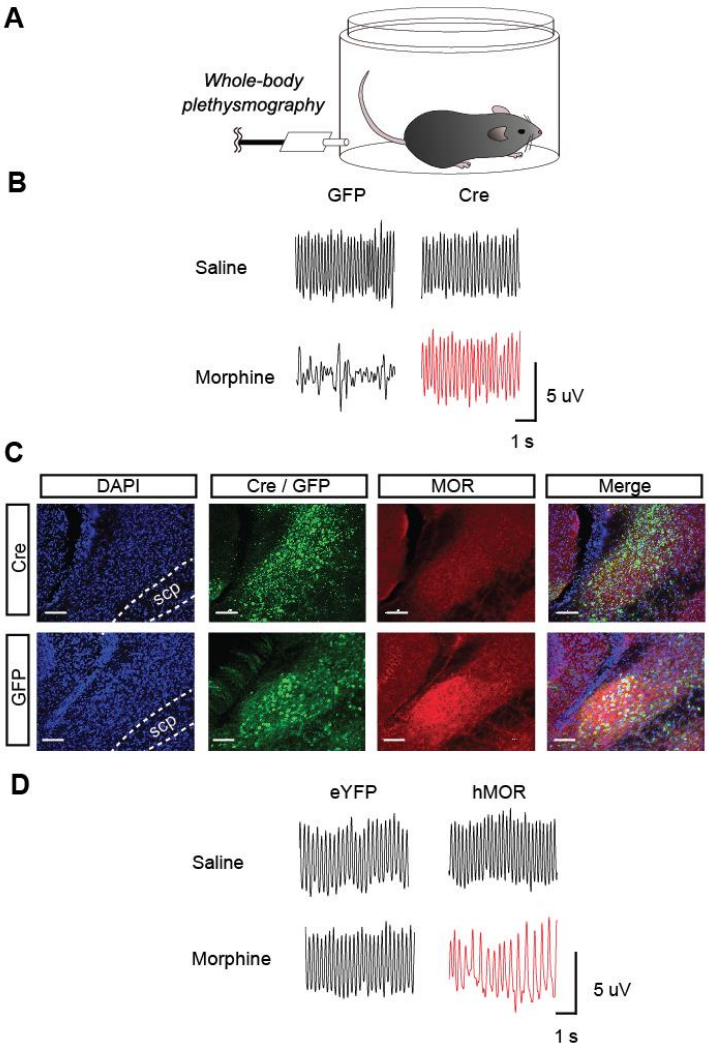


**Figure S2.** MOR signaling in the PBL is indispensable for OIRD. (**A**) Whole-body plethysmography measured respiratory parameters before and after systemic injection of saline and morphine, after conditional ablation (**B**) and rescue (**D**) of the MOR signaling in the PBL. (**B**) Example plethysmograph after saline and morphine injections into the *Oprm1*$^{fl/fl}$ mice expressing AAV-GFP and AAV-Cre-GFP in the PBL. (**C**) Confirmation of MOR deletion by MOR immunohistochemistry after stereotaxic injection of AAV-Cre-GFP and control AAV-GFP into the PBL of the *Oprm1*$^{fl/fl}$ mice. Scale bar, 100 μm. (**D**) Example plethysmograph after saline and morphine injections into the *Oprm1*$^{Cre/Cre}$ mice expressing AAV-DIO-eYFP and AAV-DIO-hMOR in the PBL.

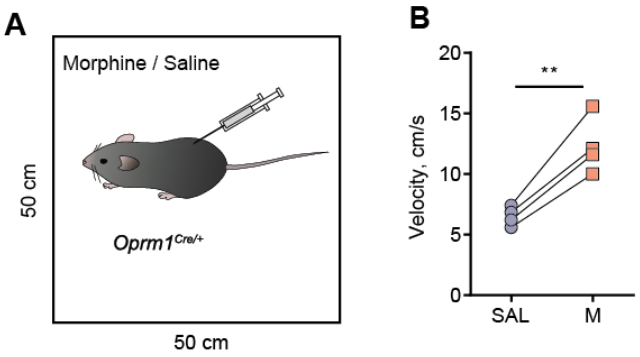


**Figure S3.** Morphine effect on locomotor activity. (**A**) Locomotor activity of *Oprm1*$^{Cre/+}$ mice after morphine (40 mg/kg, i.p.) or saline injection was measured in the open field. (**B**) Systemic morphine injection increased locomotor activity in *Oprm1*$^{Cre/+}$ mice. Paired t-test, **, $p < 0.01$.

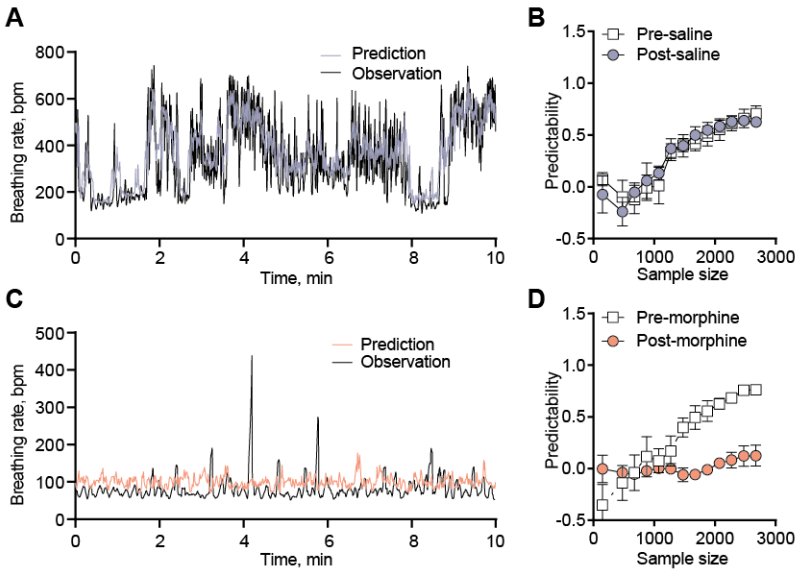


**Figure S4.** Morphine eliminated the breathing predictor. Convergent cross-mapping (CCM) prediction of breathing rate using calcium activity as inputs before and after saline (0.9%, i.p., **A** and **B**) and morphine (40 mg/kg, i.p., **C** and **D**) injection. (**A**) After saline injection, the predicted and observed breathing rate traces followed closely with each other during the 10-min example. (**B**) Model predictability increased with the sample size before and after saline injection (n = 4). (**C**) After morphine injection, the predicted and observed breathing rate traces no longer matched with each other. (**D**) Model predictability increased with the sample size before morphine injection, but the relationship was completely abolished after morphine injection (n = 4).

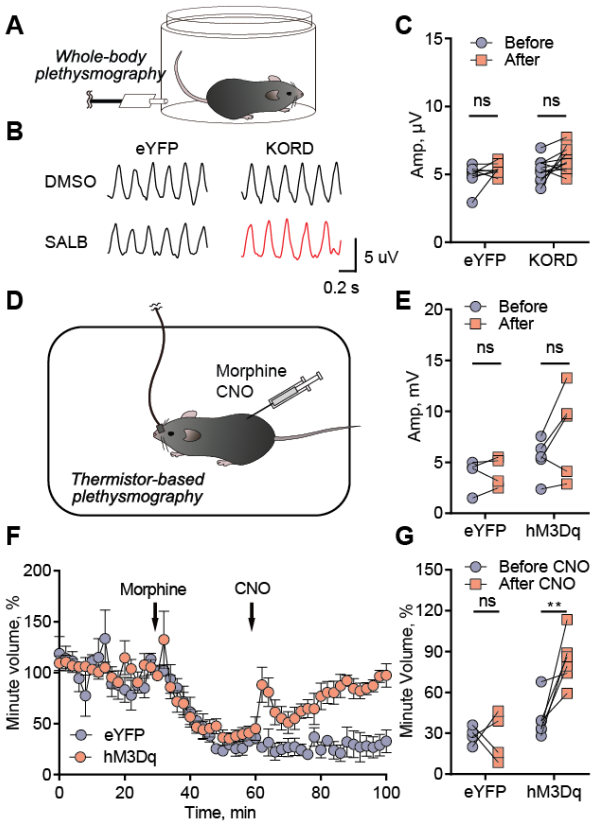


**Figure S5.** (**A**) Whole-body plethysmography was used to measure respiratory parameters before and after systemic injection of DMSO and SALB in the *Oprm1*$^{Cre/Cre}$ mice expressing AAV-DIO-eYFP and AAV-DIO-KORD in PBL$^{Oprm1}$ neurons. (**B**) Example plethysmograph after DMSO and 7.5 mg/kg SALB injections in eYFP and KORD groups. KORD-expressing animals displayed a slower respiratory rate after SALB injection compared to other groups. (**C**) Respiratory amplitude was not significantly changed before and after SALB injection, in both eYFP (n = 8) and KORD (n = 11)-expressing animals. Two-way ANOVA with Bonferroni's multiple comparison post-hoc test, ns, not significant. (**D**) Thermistor-based plethysmography was used for measuring respiration before and after systemic injection of 40 mg/kg morphine and CNO in the *Oprm1*$^{Cre/+}$ mice expressing AAV-DIO-eYFP and AAV-DIO-hM3Dq in PBL$^{Oprm1}$ neurons. (**E**) Respiratory amplitude was not significantly changed before and after CNO injection, in both eYFP (n = 5) and hM3Dq-expressing animals (n = 6). Although there was a trend of increase in the hM3Dq group, it failed to reach statistical significance. Two-way ANOVA with Bonferroni's multiple comparison post-hoc tests, ns, not significant. (**F**) Activation of PBL$^{Oprm1}$ neurons by injecting CNO (5 mg/kg, i.p.) in the hM3Dq-expressing group (n = 6) completely rescued the minute volume to baseline level after morphine-induced respiratory depression, but not in eYFP-expressing group (n = 4). (**G**) Quantitative analysis of **F** showing CNO injection significantly increased the minute volume in the hM3Dq-expressing group (n = 6), whereas failed to rescue in the eYFP-expressing group (n = 4). Two-way ANOVA with Bonferroni's multiple comparison post-hoc test. **, $p < 0.01$.

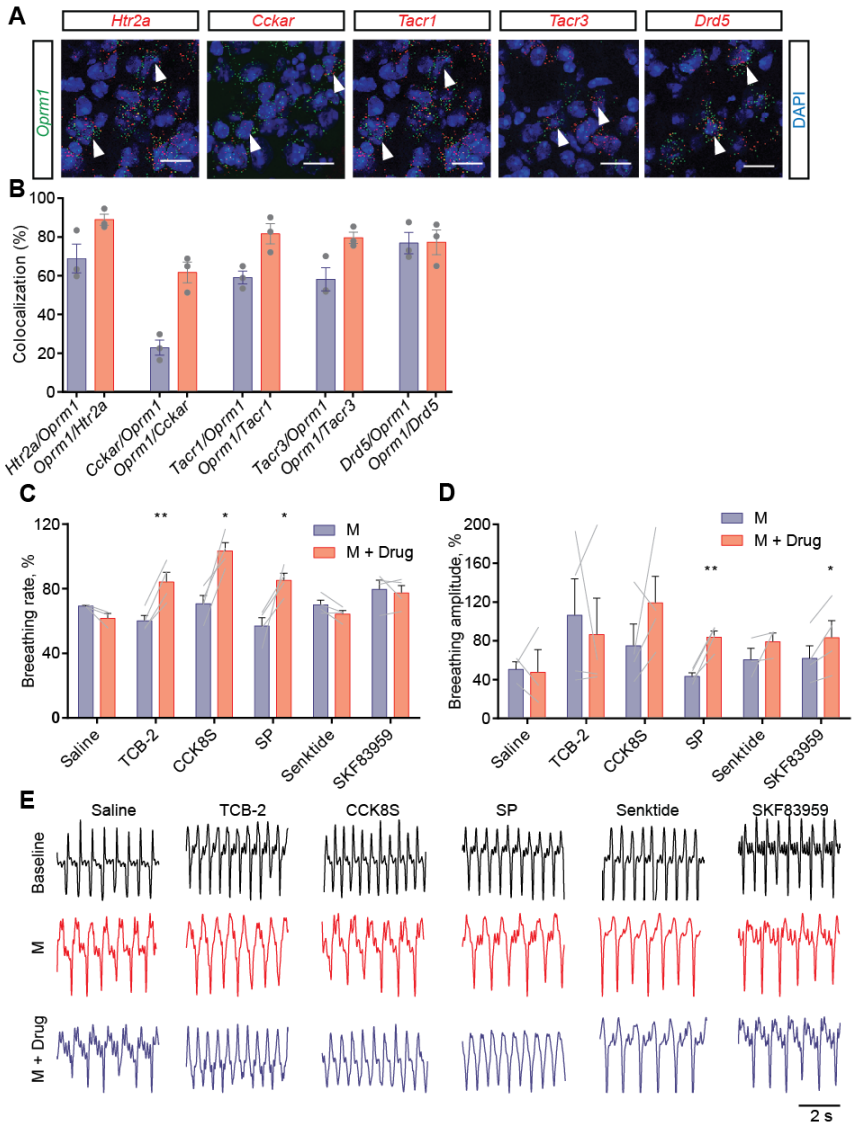


**Figure S6.** Rescuing of OIRD by activating endogenous GPCRs expressed on PBL$^{Oprm1}$ neurons. (**A**) RNA *in situ* hybridization confirms the co-expression of mRNA of *Oprm1* and five selected GPCRs, *Htr2a*, *Cckar*, *Tacr1*, *Tacr3*, and *Drd5*, in the wild type mice. Arrowheads, double-labeled cells. Scale bar, 50 μm. (**B**) Quantification of RNA *in situ* hybridization showing the colocalization of *Oprm1* and selective GPCR genes in the PBL of wild type mice (770, 539, 836, 657, 431 cells for *Htr2a*, *Cckar*, *Tacr1*, *Tacr3*, and *Drd5*, respectively). (**C-D**) Normalized breathing rate (**C**) and amplitude (**D**) before morphine injection (Baseline), 30 minutes after morphine injection (80 mg/kg, s.c., M), and 30 minutes after drug injection into the PBL (M + Drug), for all six drugs tested. Large variations in amplitude are due to the technical limitations of the piezoelectric sensor since its location is subjective to the slight movements of the animal's body. Paired t-test, *, $p < 0.05$; **, $p < 0.01$. **e** Example plethysmograph showing the breathing rhythm changes at each stage of the experiment. Note the decreased breathing rate after morphine injection and increased breathing rate after TCB-2, CCK8S, and SP injections. The exact shape of the plethysmograph varies due to the placement of the piezoelectric sensor.

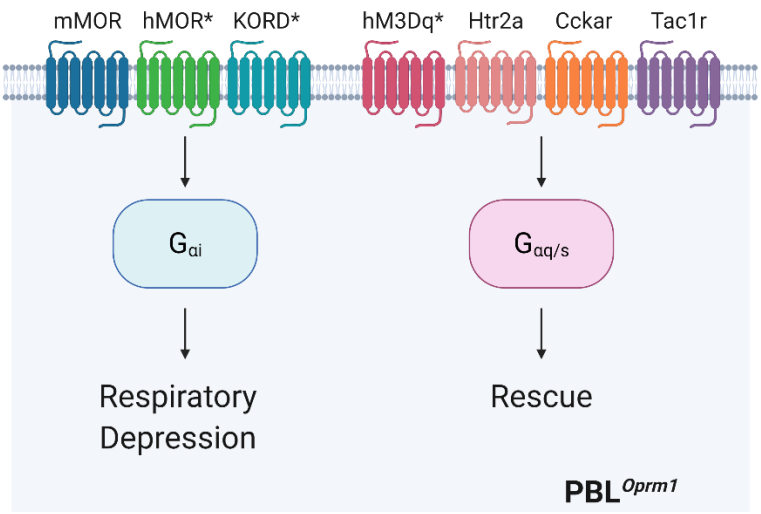


**Figure S7.** Summary of the current study. PBL$^{Oprm1}$ neurons are critical players in OIRD pathogenesis and promising therapeutic targets for treating OIRD. In intact mice, inhibition of PBL$^{Oprm1}$ neurons through $G_i$-coupled GPCRs via endogenous MOR (mMOR), human MOR (hMOR), and KOR-derived DREADD (KORD) leads to respiratory depression. In contrast, activation of these neurons via artificial (hM3Dq) or endogenous $G_{q/s}$-coupled GPCRs (Htr2a, Cckar, Tac1r) rescues OIRD. Artificial GPCRs are marked with asterisks. Created with BioRender.com.

**Supplementary Table 1. List of pharmacological agents used in the current study.**

| Drug Name | Receptor (Gene) | Receptor Family | Concentration | Solvent | Company |
|---|---|---|---|---|---|
| Naloxone | MOR (*Oprm1*) | Gi | 0.4 mg/mL (i.c., intracranial) | 0.9% saline | Somerset Therapeutics |
| Morphine | MOR (*Oprm1*) | Gi | 80 mg/kg (s.c., for anesthesia experiments);<br>10 mg/kg (i.p., for PBL-specific *Oprm1* knockout);<br>40 mg/kg (i.p., for all other experiments) | 0.9% saline | Spectrum Chemical |
| Salvinorin B (SALB) | KORD | Gi | 7.5 mg/kg (i.p.) | 0.9% saline containing 10% DMSO | Cayman Chemical |
| Clozapine-N-oxide (CNO) | hM3Dq | Gq | 5 mg/kg (i.p.) | 0.9% saline | Cayman Chemical |
| TCB-2 | 5-$HT_{2A}$ (*Htr2a*) | Gq | 1 mg/mL (i.c.) | 0.9% saline | Tocris Bioscience |
| CCK Octapeptide, sulfated (CCK8S) | $CCK_1R$ (*Cckar*) | Gq | 1 mg/mL (i.c.) | 0.9% saline | Abcam |
| Substance P | $NK_1R$ (*Tacr1*) | Gq, Gs | 1 mg/mL (i.c.) | 0.9% saline | Cayman Chemical |
| Senktide | $NK_3R$ (*Tacr3*) | Gq | 1 mg/mL (i.c.) | 0.9% saline | Cayman Chemical |
| SKF-83959 | $D_5R$ (*Drd5*) | Gs | 1 mg/mL (i.c.) | 0.9% saline containing 5% DMSO | Tocris Bioscience |

**Supplementary Table 2. Key Resources Table**

| Type | Designation | Source or reference | Identifiers |
|---|---|---|---|
| Mouse strains | Oprm1-Cre:GFP | Laboratory of Dr. Richard Palmiter | N/A |
| | Wild type C57BL/6J | Jackson Laboratory | Stock No. 000664 |
| | RiboTag *Rpl22*$^{HA/HA}$ | Jackson Laboratory | Stock No. 011029 |
| | Ai14 *Gt(ROSA)26Sor*$^{tm14(CAG-tdTomato)Hze}$ | Jackson Laboratory | Stock No. 007914 |
| Virus | AAVDJ-CAG-Cre-GFP | Salk Institute Viral Vector Core | N/A |
| | AAVDJ-CAG-GFP | Salk Institute Viral Vector Core | N/A |
| | AAV-hSyn-DIO-mCherry-T2A-FLAG-hOprm1 | Laboratory of Dr. Matthew Banghart | N/A |
| | AAV1-syn-FLEX-jGCaMP7s-WPRE | Addgene | Addgene# 104491 |
| | AAVDJ-EF1a-DIO-hM3D(Gq)-mCherry | Salk Institute Viral Vector Core | Addgene# 50460 |
| | AAV-DIO-KORD-mCitrine | Laboratory of Dr. Richard Palmiter | N/A |
| | AAV1-DIO-eYFP | Laboratory of Dr. Richard Palmiter | N/A |
| Antibodies | Anti-hemagglutinin1.1, mouse (1:1000) | BioLegend | RRID AB_2565335 |

| | | | |
|---|---|---|---|
| | Anti-GFP, chicken (1:1000) | Aves Labs | RRID AB_2307313 |
| | Anti-MOR, rabbit (1:1000) | ImmunoStar | RRID AB_572251 |
| | Alexa Fluor® 647-conjugated Donkey Anti-Mouse IgG (1:1000) | Jackson ImmunoResearch Laboratories | RRID AB_2340863 |
| | Alexa Fluor® 488-conjugated Donkey Anti-Chicken IgY (1:1000) | Jackson ImmunoResearch Laboratories | RRID AB_2340375 |
| | Alexa Fluor® 647-conjugated Donkey Anti-Rabbit IgG (1:1000) | Jackson ImmunoResearch Laboratories | RRID AB_2492288 |
| RNAscope probes | Oprm1 | Advanced Cell Diagnostics | 315841 |
| | Htr2a | Advanced Cell Diagnostics | 401291 |
| | Cckar | Advanced Cell Diagnostics | 313751 |
| | Drd5 | Advanced Cell Diagnostics | 494411 |
| | Tacr3 | Advanced Cell Diagnostics | 481671 |
| | Tacr1 | Advanced Cell Diagnostics | 428781 |
| | Cre | Advanced Cell Diagnostics | 402551 |
| | Slc17a6 | Advanced Cell Diagnostics | 319171 |
| | Slc32a1 | Advanced Cell Diagnostics | 319191 |
| Chemicals | FluoSpheres 540/560 (10% v/v) | Thermo Fisher | Cat# F8809 |

| | | | |
|---|---|---|---|
| | Cholera Toxin Subunit B-555 | Invitrogen | Cat# C34776 |
| | Naloxone | Somerset Therapeutics | Cat# 70069007110 |
| | Morphine | Spectrum Chemical | Cat# M1167 |
| | TCB-2 | Tocris Bioscience | Cat# 2592 |
| | CCK Octapeptide, sulfated | Abcam | Cat# ab120209 |
| | Substance P | Cayman Chemical | Cat# 24035 |
| | Senktide | Cayman Chemical | Cat# 16721 |
| | SKF-83959 | Tocris Bioscience | Cat# 2074 |
| | Clozapine N-oxide | Cayman Chemical | Cat# 16882 |
| | Salvinorin B | Cayman Chemical | Cat# 11488 |
| | 2-methylbutane | Fisher Chemical | Cat# O35514 |
| Software | Doric Neuroscience Studio | Doric Lenses | N/A |
| | RStudio | RStudio | Version 1.2.5001 |
| | rEDM | https://cran.r-project.org/web/packages/rEDM/ | Version 0.7.2 |
| | rEDM | https://ha0ye.github.io/rEDM/ | Version 0.7.4 |
| | LabChart | ADInstruments | Version 8 |
| | BZ-X viewer | Keyence | N/A |
| | OlyVIA | Olympus Life Science | N/A |
| | PRISM | GraphPad Software | Version 6 |

| | | | |
|---|---|---|---|
| | Illustrator | Adobe | Version CS6 and CC2018 |

121

122